Active Efficient Coding Explains the Development of Binocular Vision and its Failure in Amblyopia

Samuel Eckmann[a,b,1], **Lukas Klimmasch**[a,b], **Bertram E. Shi**[c], **and Jochen Triesch**[a,b,1]

[a]Frankfurt Institute for Advanced Studies, Frankfurt am Main, Germany; [b]Department of Computer Science and Mathematics, Goethe University, Frankfurt am Main, Germany; [c]Department of Electronic and Computer Engineering, Hong Kong University of Science and Technology, Clear Water Bay, Hong Kong

The development of vision during the first months of life is an active process that comprises the learning of appropriate neural representations and the learning of accurate eye movements. While it has long been suspected that the two learning processes are coupled, there is still no widely accepted theoretical framework describing this joint development. Here we propose a computational model of the development of active binocular vision to fill this gap. The model is based on a new formulation of the *Active Efficient Coding* theory, which proposes that eye movements, as well as stimulus encoding, are jointly adapted to maximize the overall coding efficiency. Under healthy conditions, the model self-calibrates to perform accurate vergence and accommodation eye movements. It exploits disparity cues to deduce the direction of defocus, which leads to coordinated vergence and accommodation responses. In a simulated anisometropic case, where the refraction power of the two eyes differs, an amblyopia-like state develops, in which the foveal region of one eye is suppressed due to inputs from the other eye. After correcting for refractive errors, the model can only reach healthy performance levels if receptive fields are still plastic, in line with findings on a critical period for binocular vision development. Overall, our model offers a unifying conceptual framework for understanding the development of binocular vision under healthy conditions and in amblyopia.

efficient coding | active perception | amblyopia | vergence | accommodation

Our brains are responsible for 20% of our energy consumption (1), therefore, organizing neural circuits to be energy efficient may provide a substantial evolutionary advantage. One means of increasing energy efficiency in sensory systems is to attune neural representations to the statistics of sensory signals. Based on this *Efficient Coding Hypothesis* (2), numerous experimental observations in different sensory modalities have been explained (3, 4). For instance, it has been shown that receptive field properties in the early visual pathway can be explained through models that learn to efficiently encode natural images (5, 6). These findings have extended classic results showing that receptive field shapes in visual cortex are highly malleable and a product of the organism's sensory experience (7–10).

Importantly, however, animals can shape the statistics of the sensory inputs through their behavior (Fig. 1). This gives them additional degrees of freedom to optimize coding efficiency by jointly adapting their neural representations and behavior. This idea has recently been advanced as *Active Efficient Coding* (11, 12). It can be understood as a generalization of the efficient coding hypothesis (2) to active perception (13). Along these lines, *Active Efficient Coding* models have been able to explain the development of visual receptive fields and the self-calibration of smooth-pursuit and vergence eye movements (11, 12). This has been achieved by optimizing the neural representation of the sensory signal statistics, while

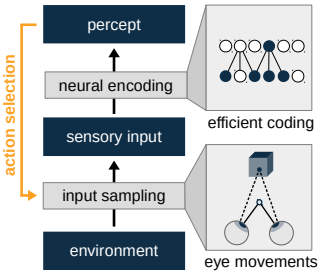

Fig. 1. The action-perception loop in *Active Efficient Coding*. The sensory input is obtained by sampling input signals from the environment, e.g., via eye movements. A percept is formed by neural encoding which drives the selection of actions and thereby shapes the sampling process. Therefore, perception depends on both, neural encoding and active input sampling. Classic efficient coding theories do not consider the active sampling component (orange).

simultaneously, via eye movements, optimizing the statistics of sensory signals themselves, for maximal coding efficiency.

In our formulation of *Active Efficient Coding*, we maximize coding efficiency as measured by the Shannon mutual information $I(R, C)$ between the retinal stimulus represented by retinal ganglion cell activity R and its cortical representation C under a limited resource constraint. The mutual information can be decomposed as:

$$I(R, C) = \mathcal{H}(R) - \mathcal{H}(R|C), \qquad [1]$$

where $\mathcal{H}(R)$ is the entropy of the retinal stimulus and $\mathcal{H}(R|C)$ its conditional entropy given the cortical representation.

Prior formulations focused on minimizing the conditional term $\mathcal{H}(R|C)$ only (6) (or equivalently maximizing $-\mathcal{H}(R|C)$, see SI Appendix). $\mathcal{H}(R|C)$ is a measure of the information that is lost, i.e., not represented in the cortical encoding. The limitation of this prior formulation is that the unconditioned input signal entropy is an upper bound on the conditioned

Significance Statement

Brains must operate in an energy-efficient manner. The efficient coding hypothesis states that sensory systems achieve this by adapting neural representations to the statistics of sensory input signals. Importantly, however, these statistics are influenced by the organism's behavior and how it samples information from the environment. Therefore, optimal performance requires jointly optimizing neural representations and behavior, a theory called *Active Efficient Coding*. Here we test the plausibility of this theory by proposing a computational model of the development of binocular vision. The model explains the development of accurate binocular vision under healthy conditions. In the case of refractive errors, however, the model develops an amblyopia-like state and suggests conditions for successful treatment.

SE, BS and JT designed the study. SE performed the simulations and analyzed the results. LK helped to implement the suppression model. SE and JT wrote the first draft of the paper.

The authors declare no conflict of interest.

[1]Correspondence: eckmann@fias.uni-frankfurt.de, triesch@fias.uni-frankfurt.de

entropy, i.e.,

$$\mathcal{H}(R|C) \leq \mathcal{H}(R). \qquad [2]$$

Thus, an active agent that can control the entropy in the input signal, e.g., via accommodation, could minimize $\mathcal{H}(R|C)$ by minimizing $\mathcal{H}(R)$, e.g., by defocusing or closing the eyes altogether. In the free-energy and predictive processing literature, this is known as the "dark room problem" (14, 15). Prior formulations avoided this problem by lower bounding $\mathcal{H}(R)$, e.g., by assuming perfect focus and by randomly switching images between fixations, simulating saccades to new areas of the visual scene.

In our formulation, maximizing I(R, C) is achieved by maximizing $\mathcal{H}(R)$ and minimizing $\mathcal{H}(R|C)$ simultaneously, thus circumventing this problem. We demonstrate this approach through a concrete model of the development of binocular vision including the simultaneous calibration of vergence and accommodation control.

Indeed, newborns have difficulties bringing objects into focus and cannot yet verge their eyes properly (16). How infants manage to self-calibrate their control mechanisms while interacting with their visual environment is currently unknown.

Additionally, in certain medical conditions, the calibration of vergence and accommodation control is hindered. For example, anisometropia describes a difference in the refractive error between the eyes. If not corrected early during development, this can evoke amblyopia: a disorder of the developing visual system that is characterized by an interocular difference in visual acuity that is not immediately resolved by refractive correction. Amblyopia can be associated with a loss of stereopsis and in severe cases leads to monocular blindness (17). Furthermore, vergence and accommodation eye movements are either less accurate or completely absent (18, 19).

Although there have been recent advances in the treatment of amblyopia (20, 21), existing treatment methods do not lead to satisfactory outcomes in all patients. This is aggravated by the fact that treatment success strongly depends on the stage of neural circuit maturation (20). When young patients are still in a critical period of circuit plasticity (10), they often recover after refractive errors are corrected, while adults mostly remain impeded (22, 23).

The above findings are all readily explained by our model. Under healthy conditions, our agent develops accurate vergence and accommodation eye movements. When the model is impaired due to strong monocular hyperopia, we observe that one eye suppresses the other and an amblyopia-like state develops. We show that this is due to the abnormal development of binocular receptive fields in the model and demonstrate that healthy binocular vision is regained when the receptive fields readapt after refraction correction. However, if the sensory encoding is no longer plastic and does not adapt to the changes in the visual input statistics, suppression prevails. Overall, our model suggests that coding efficiency may provide a unifying explanation for the development of binocular vision.

Model Formulation. The *Active Efficient Coding* model we propose has a modular structure (Fig. 2). A cortical coding module models the learning of an efficient representation C of the binocular retinal representation R. At the same time, an accommodation reinforcement learning module maximizes $\mathcal{H}(R)$ and a vergence reinforcement learning module minimizes

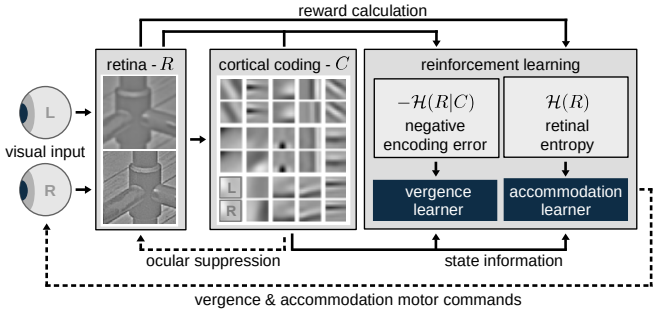

Fig. 2. Model architecture with solid arrows representing the flow of sensory information and dashed arrows representing the flow of control commands. Only one cortical coding scale is shown. Sampled input images with given defocus blur and disparity are whitened at the retinal stage R (left). Thereafter, they are encoded by a set of binocular neurons which represents the cortical encoding C. In the healthy case, without refractive errors, receptive fields are mostly binocular and tuned to disparities near zero (center) (see Fig. S6). The state information passed the two reinforcement learning modules (right) that control vergence and accommodation commands is the population response of the cortical neurons. Accommodation commands are learned to maximize the retinal entropy. Vergence commands are learned to minimize encoding error. An ocular suppression mechanism adjusts left and right eye contrasts before encoding. For details, see Methods and SI Appendix.

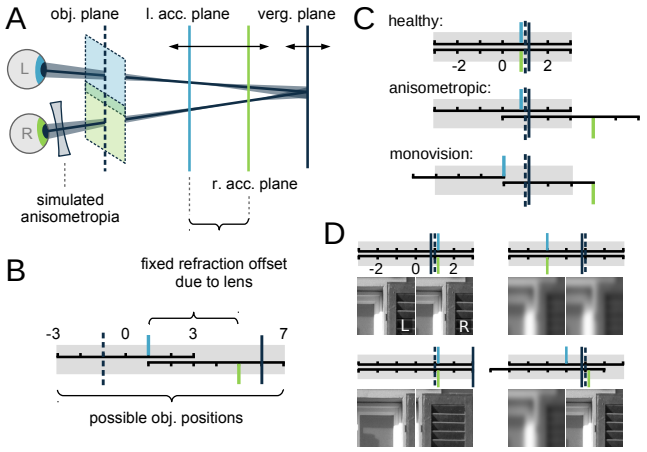

Fig. 3. Input sampling from the environment. *(A)* Object position, eye-focus, and eye fixation at different distances are represented as different plane positions. *(B)* Abstraction of *A*. The gray horizontal bar indicates the range where objects are presented during the simulation and also indicates the fixation range, i.e., possible vergence plane positions. Horizontal axes indicate reachable accommodation plane positions for the left (light blue) and right (green) eye. Note that when the stimulus is placed at, e.g., position 0 it cannot be focused by the right eye in this example. Accommodation and vergence errors are measured as the distance between the respective planes and the object position, in a.u. *(C)* Position range of accommodation and vergence planes under different conditions. Same scheme as in *B*. *(D)* Examples of retinal input images for different plane position configurations. For better visibility, disparity shifts and defocus blur are increased compared to actual values.

$\mathcal{H}(R|C)$ (see Eq. 1). All three modules are plastic and adjust simultaneously in response to changes in the sensory input statistics. The exact choice of the algorithms is not important for the model to function. In fact, different cortical coding and reinforcement learning models have been successfully applied in previous *Active Efficient Coding* models (24, 25).

Our model comprises an observer looking at a textured planar object. The object is sampled by the two eyes for ten subsequent iterations which constitute one fixation. After each fixation, a new object is presented at a new, random distance. The retinal images are rendered based on the positions of the accommodation, vergence, and object planes (Fig. 3).

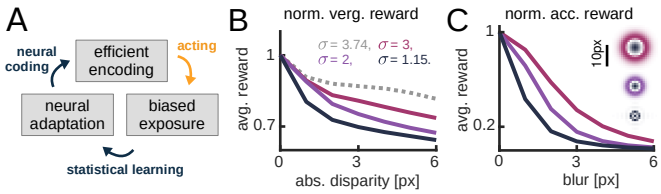

Fig. 4. The feedback loop of *Active Efficient Coding* and reward dependencies. *(A)* Positive feedback loop of *Active Efficient Coding*. An efficiently encoded stimulus is preferred over other stimuli (acting). Therefore, the sensory system is more frequently exposed to the stimulus and neural circuits adapt to reflect this overrepresentation (statistical learning) which further increases encoding efficiency (neural coding). *(B)* Normalized vergence reward for different disparity distributions and neural populations. Averaged over 300 textures. The receptive fields of 300 neurons adapted to different distributions of input disparities with color-coded standard deviations. Gray: unbiased/uniform, pink & purple: laplacian distributed, dark blue: model trained under healthy conditions). In each case, stimuli seen at zero disparity produce the highest vergence reward, i.e., the most efficient encoding. This advantage is even more pronounced when small disparities have been encountered more frequently, i.e., for smaller σ. *(C)* Normalized accommodation reward for different whitening filters. Zero disparity input yields the highest accommodation reward, independent of the size of the whitening filter. However, smaller whitening filters have a stronger preference for focused input. The smallest filter (dark blue) was used for the simulation (see SI Appendix for details).

The inputs are whitened, contrast adjusted by an interocular suppression mechanism, and then binocularly encoded by a population of cortical neurons. The reinforcement learning modules control the retinal input of the next iteration by shifting accommodation and vergence planes along the egocentric axis (Fig. 3).

Cortical Encoding. In our model, the cortical population activity represents the binocular 'percept' based on which behavioral commands are generated (compare Fig. 1, top). The cortical encoding comprises two efficient coders: One for fine details in the foveal region and one for the periphery that receives a low-pass filtered input. The encoding depends on the receptive fields of the activated neurons, which resemble those of simple cells in the visual cortex (6) (Fig. S6). Their tuning characteristics adjust online to minimize the conditional entropy $\mathcal{H}(R|C)$, which can be understood as a measure of encoding error. Thus, the receptive fields reflect the recent stimulus statistics (26) (see Methods & SI Appendix for details).

Vergence Learning. The vergence reinforcement learner also minimizes the conditional entropy $\mathcal{H}(R|C)$, i.e., the encoding error. Therefore, stimuli are favored that can be most accurately encoded with the current set of receptive fields. This leads to a self-reinforcing feedback loop (Fig. 4*A*). When a stimulus can be more efficiently encoded than competing stimuli, it becomes favored by the reinforcement learning agent. As a result, the input statistics that the agent is exposed to, change such that the favored stimulus becomes overrepresented. The cortical representation reflects this change by adjusting the number of receptive fields that are selective for the overrepresented stimulus or slight variations thereof, which further increases the efficiency of its encoding (Fig. 4*B*). Thus, a small bias can be magnified until it dominates alternative choices. In our model, we approximate $\mathcal{H}(R|C)$ with the difference between the retinal and cortical squared activity, i.e., $||R||^2 - ||C||^2$ (see Methods & SI Appendix).

Accommodation Learning. In our model, the entropy of the retinal response $\mathcal{H}(R)$ (Eq. 1) is maximized via the accommodation reinforcement learning module. We assume the spatial frequency tuning of retinal ganglion cells to be static and thus independent of the distribution of spatial frequencies in the retinal input as suggested by deprivation experiments (9, 27, 28). Yet, we find that the exact receptive field shape does not matter for the model to favor focused input (Fig. 4*C*).

The entropy $\mathcal{H}(R)$ is approximated with the squared activity of the retinal representation $||R||^2$ (see Methods & SI Appendix).

Suppression Model. We employ a basic interocular suppression model (Fig. 5) to describe dynamic contrast modulation based on the ocular balance of the input encoding. If mostly right (left) monocular receptive fields are recruited during cortical encoding, the contrast of the left(right) eye input gets suppressed in subsequent iterations. This is in agreement with reciprocal excitation of similarly tuned neurons in visual cortex (29, 30). At the same time, the total input energy is kept balanced to ensure similar activity levels for monocular and binocular visual experience as observed experimentally at high contrast levels (31–33) (see Methods & SI Appendix). This leads to a self-reinforcing suppression loop when left and right eye inputs are dissimilar (Fig. 5*B*).

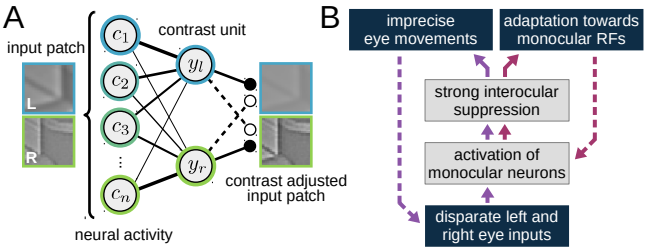

Fig. 5. Interocular suppression model. *(A)* When mostly right(left) monocular neurons c_j are activated to encode an input patch, the right(left) contrast unit $y_r(y_l)$ is excited and the left(right) retinal image is suppressed. Dashed(solid) lines indicate inhibitory(excitatory) interactions. Connection strength is represented by line thickness. We model interocular suppression as being scale specific, i.e., when the high-resolution foveal region of the left eye is suppressed, the low-resolution periphery of the left eye may still provide unattenuated input (see Methods & SI Appendix). *(B)* Feedback loops of the suppression model. Disparate inputs lead to preferential recruitment of monocular neurons which results in interocular suppression. This impedes precise eye movements and leads to even more disparate input (purple, left loop). Suppression alters the ocular contrast balance of the input patch. Therefore, receptive fields (RFs) adapt by becoming more monocular, which makes future suppression likelier (red, right loop). Dashed lines indicate feedback that affects future input processing.

Results

Active Efficient Coding Leads to Self-calibration of Active Binocular Vision. In the healthy condition without refractive errors, the model learns to perform precise vergence eye movements (Fig. 6*A* & SI Appendix, Fig. S8*A* & S9*A*) and most neurons develop binocular receptive fields (see examples in Fig. 2 & SI Appendix, Fig. S6). This is not due to artificially introducing a bias for zero disparity during initialization of the model. When receptive fields are adapted to a uniform input disparity distribution, the encoding of zero disparity input is still most efficient (Fig. 4*B*). Due to the overlap of the left and right eye visual field, the binocular input information $\mathcal{H}(R)$ for zero disparity input is smaller than for non-zero disparity input, where the combined field of view of both eyes is larger and, therefore, visual input more redundant. In the case of an

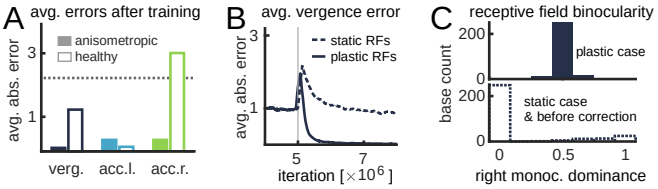

Fig. 6. Model performance. *(A)* Average absolute vergence and accommodation errors after training under healthy and anisometropic conditions. The dashed line indicates the expected average vergence error when accommodation planes are moved randomly under healthy conditions. *(B)* Vergence performance of formerly anisometropic model after correction of all refractive errors at iteration 5×10^6 (vertical gray line). The (dotted)solid line indicates the model with (non-)plastic receptive fields (RFs). The initial increase in the vergence error is due to the recalibration of the reinforcement learning module. *(C)* Histogram of foveal monocular dominance $d_{(\cdot,r)}$ before and after refractive error correction (see Methods & SI Appendix for details).

unbiased encoder, by definition, equal amounts of information $I(R, C)$ are encoded, independent of the input disparity. Then, the encoding efficiency $-\mathcal{H}(R|C) = I(R, C) - \mathcal{H}(R)$ is highest when the two eyes are aligned, as it yields the lowest input entropy $\mathcal{H}(R)$, which initializes the feedback loop (Fig. 4*A*, SI Appendix Fig. S7).

Accommodation performance is highly accurate as well. This is due to the edge-enhancing nature of retinal ganglion cell receptive fields. With their center-surround shape, they are selective for sharp contrasts and respond poorly when out of focus input is presented (Fig. 4*C*). For sharper input, the range of responses across the population, and thus the response entropy, increases (SI Appendix, Fig. S5 & S4).

Furthermore, accurate accommodation is achieved without obvious sign cues: in our simplified visual environment, defocus blur is independent of whether an eye focuses behind or in front of the object (SI Appendix, Fig. S1). Also, neither chromatic nor other higher-order aberrations are provided in our model, which could help to steer focus in the right direction (34, 35). Instead, the model capitalizes on the simultaneous movement of the vergence and accommodation planes such that the sign of defocus is inferred from disparity cues (SI Appendix, Fig. S11). We further examined this entanglement under abnormal input conditions, e.g. when simulated lenses were placed in front of the eyes of an agent trained under healthy conditions. We find the responses of the model to qualitatively agree with experimental results (36, 37) (SI Appendix, Fig. S12).

Anisometropia drives model into amblyopic state. To test how the model evolves under abnormal rearing conditions, we simulated an anisometropic case by adding a simulated lens in front of the right eye such that it became hyperopic and was unable to focus objects at close distances (Fig. 3*C*, center). Therefore, unlike the healthy case, where neither eye is favored over the other, in the anisometropic case, the impaired eye receives systematically more defocused input. Hence, its input entropy is decreased (compare SI Appendix, *Accommodation Reward* section). Cortical receptive fields reflect this imbalance and become more monocular, favoring the unimpaired eye (compare Fig. 6*C*, bottom and Fig. S6, top, center). The combined effect of imbalanced input and adapting receptive fields results in a positive feedback loop that drives the model into an amblyopia-like state (Fig. 5*B*). Foveal input from the hyperopic eye becomes actively suppressed (SI Appendix, Fig. S10*A*) while the low-resolution peripheral input is unaffected and still provides binocular information such that a coarse control of vergence is maintained (Fig. 6*A* and SI Appendix, Fig. S8*B* & S9*B*). This results in stable binocular receptive fields in the periphery (Fig. S6, bottom, center) which provide enough information for coarse stereopsis as observed in experiments (38–40). Accommodation adapts such that the stimulus is continuously tracked with the unimpaired eye (SI Appendix, Fig. S9).

When both eyes were similarly impaired but with opposite sign of the refractive error (Fig. 3*C*, bottom), receptive fields still become more monocular but both eyes are equally disadvantaged (Fig. S6, top, right). As a result, the relatively more myopic eye is used for near and the relatively less myopic eye for distant vision (SI Appendix, Fig. S13*C*) and the respective other, defocused eye is suppressed. This configuration is similar to monovision, which results from a treatment method for presbyopia, where the ametropic condition is achieved via optical lenses or surgery (41).

Early but not late refractive correction rescues binocular vision. To test if the anisometropic model can recover from amblyopia upon correction of the refractive error, we first trained a fully plastic model under anisometropic conditions until it reached stable performance. Then, all refractive errors were corrected. When the receptive fields were fixed after the refractive error was corrected, receptive fields remained monocular and the model did not recover from the amblyopic state. Instead, it maintained a high level of vergence error (Fig. 6*B*, dotted line). In contrast, when receptive fields remained plastic and could adapt to the changed input statistics the strong suppression of the formerly impaired eye was restored to lower values (Fig. 6*B* and SI Appendix, Fig. S10*B*, solid lines). This was due to a shift from monocular to binocular receptive fields as a result of the changed input statistics (Fig. 6*C*). This is in line with a large body of evidence suggesting that limited cortical plasticity prevents recovery from amblyopia after the correction of refractive errors (10, 20, 21). Furthermore, it predicts that therapies reinstating visual cortex plasticity should be effective.

Discussion

We have shown how simultaneously optimizing both behavior and encoding for efficiency leads to the self-calibration of active binocular vision. Specifically, our model, which is based on a new formulation of the *Active Efficient Coding* theory, accounts for the simultaneous development of vergence and accommodation. Under healthy conditions, the model develops accurate vergence and accommodation eye movements. For a simulated anisometropia, however, where one eye suffers from a refractive error while the other eye is unaffected, it develops into an amblyopia-like state with monocular receptive fields and loss of fine stereopsis. Recovery from this amblyopia-like state is only possible if receptive fields in the model remain plastic, matching findings of a critical period for binocular development (10).

The simple logic behind the model's suppression mechanism is that every neuron suppresses input that is incongruent to its own receptive field (32, 33). This proved sufficient to account for the development of an amblyopia-like state, with mostly monocular receptive fields in the representation of the fovea. More sophisticated suppression models could be incorporated in the future (42, 43), but we do not expect them to change

the conclusions from the present model. However, a topic of current interest is how suppression develops during disease and treatment, e.g., with the standard patching method (44). A better understanding of the role of suppression in amblyopia could lead to improved therapies in the future.

Previous computational models have focused on either the development of disparity tuning or the development of vergence and accommodation control, but have failed to capture their rich interdependence (26, 45–47). For example, a model by Hunt et al. (26) explained how disparity tuning may emerge through sparse coding and how alternate rearing conditions could give rise to systematic differences in receptive field properties, but their model completely neglected vergence and accommodation behavior. Conversely, others have presupposed populations of cells readily providing error signals for vergence and accommodation control without explaining their developmental origin (45, 47). Therefore, previous models have failed to explain how the visual system solves the fundamental "chicken and egg" problem of disparity tuning and eye movement control: the development of fine disparity detectors requires the ability to accurately focus and align the eyes, which in turn relies on the ability to detect fine disparities. Our *Active Efficient Coding* model solves this problem through the positive feedback loop between disparity tuning, which facilitates the control of eye movements, and improved accommodation and vergence behavior, which enhances the representation of fine disparities. Through this mechanism, visual representations come to reflect the image statistics produced by the system's own behavior (48).

While we have focused on the development of active binocular vision including accommodation and vergence control, our formulation of *Active Efficient Coding* is very general and could be applied to many active perception systems across species and sensory modalities. *Active Efficient Coding* is rooted in classic efficient coding ideas (2–6), of which predictive coding theories are special examples (49–51). Classic efficient coding does not consider optimizing behavior, however. Friston's Active Inference approach does consider the generation of behavior in a very general fashion. There, motor commands are generated to fulfill sensory predictions. In our new formulation of *Active Efficient Coding*, motor commands are learned to maximize the mutual information between the sensory input and its cortical representation. This implies maximizing the amount of sensory information sampled from the environment and avoids the problem of deliberately using accommodation to defocus the eyes, or closing the eyes altogether, to make the sensory input easy to encode and/or predict.

Materials and Methods

Input Image Rendering. We used 300 grayscale converted natural images of the 'man-made' category from the McGill Database (52). One image was presented at a random position (see Fig. 3*A* and *B*) during one fixation, i.e., 10 subsequent iterations, before the next image and position were randomly selected for the next fixation. For the foveal scale, two retinal images of size 72×72 pixels were cropped from the center of the original image (SI Appendix, Fig. S3). For every distance unit between vergence and object plane, the left(right) retinal image was shifted 1px to the left(right). A Gaussian blur filter was applied to the left and the right eye image where the standard deviations depended linearly on the distance between object and accommodation planes. 1 a.u. distance equals 0.8 px of standard deviation (SI Appendix Text and Fig. S1 & Fig. S2). Errors were measured in a.u. as distances to the object plane. For a second, peripheral scale, two 160×160 px windows were cropped from the center of the original image (see SI Appendix, Fig. S3).

Input processing. The left and right retinal input images were whitened as described by Olshausen and Field (6). For each scale, images were cut and merged into 81 binocular patches of size 2×8×8 px, where the peripheral scale was downsampled with a Gaussian pyramid by a factor of 4 (see SI Appendix, Fig. S3). Patches were normalized to zero mean intensity and subsequently encoded with the matching pursuit algorithm (53), where we recruited $N = 10$ out of 300 cortical neurons with receptive fields b_i in order to reduce the reconstruction error $||S||^2$, i.e., the energy of the residual S_n after $n = N$ encoding steps (see SI Appendix). Here, $||\cdot||$ is the Euclidean norm.

$$S_N = R - \hat{R}_N \equiv R - \sum_{k=1}^{N} c_{i_k} b_{i_k},$$

$$i_k = \underset{j}{\operatorname{argmax}} \left(|c_{j_k}| \right), \quad c_{jl} = \langle b_j, S_{l-1} \rangle,$$

where R is the retinal input patch and $\hat{R}_N$ its estimate based on the cortical responses C, i.e., the neural activities after encoding. After each encoding, receptive fields were updated through gradient descent on the reconstruction error $||S||^2$ such that their tuning reflects the current input statistics (see SI Appendix). Foveal and peripheral scale were encoded separately by their own cortical coders and neurons.

Reinforcement Learning. We used two separate natural actor critic reinforcement learners (54) to control the accommodation planes and the vergence plane, respectively. Possible actions correspond to shifts in the respective plane positions in steps of [-2, -1, 0, 1, or 2] (compare Fig. 3). The state information for both reinforcement learners are the patch-averaged squared responses of the foveal and the peripheral scale neurons of both cortical coders (see SI Appendix). This can be understood as a model for complex cells in primary visual cortex (55, 56).

Approximating Mutual Information. Rewards for the reinforcement learners are based on the squared response after whitening and cortical encoding, respectively. Together this can be understood as an empirical estimate of the mutual information between the whitened response R and cortical response C:

$$I(R, C) = \mathcal{H}(R) - \mathcal{H}(R|C),$$

where the conditional entropy $\mathcal{H}(R|C)$, is upper bounded by the reconstruction error $||S||^2$ (see SI Appendix). Due to the 'energy conservation' property of the matching pursuit algorithm (53), the energy of the residual image is equal to the energy of the retinal representation minus the energy of the cortical representation, i.e.,

$$-||S||^2 = -\left(||R||^2 - ||C||^2\right) = ||C||^2 - ||R||^2.$$

Therefore, we take the difference between cortical and retinal response energy as the reward for the vergence learner.

For the accommodation learner, we maximize the squared whitened response, i.e., $||R||^2$. This is equal to maximizing a lower bound on the entropy $\mathcal{H}(R)$ which holds for a large class of unimodal distributions (57) (see SI Appendix).

Vergence and accommodation rewards were normalized online to zero mean and unit variance intensity (see SI Appendix).

Suppression Mechanism. There are two separate suppression modules, one per scale, that adjust the contrast of left and right input image (see Fig. 5). We introduce a contrast measure $x_k, k \in \{l, r\}$ that gives an estimate of the amount of left(right) monocular input over the previous iterations.

$$x_k(t) = \left\langle \sum_i \left(\frac{c_i^2}{\sum_j c_j^2} \right) d_{(i,k)} \right\rangle_{t,\tau}.$$

The monocular dominance of each neuron $d_{(i,k)}$ is weighted with its relative activation $c_i^2 / \sum_j c_j^2$. Here, $\langle \cdot \rangle_{t,\tau}$ is the exponential moving average over time with decay constant $\tau = 10$ (see SI Appendix). The monocular dominance is defined as:

$$d_{(i,k)} = \frac{||b_{(i,k)}||}{||b_{(i,k)}|| + ||b_{(i,\bar{k})}||}, \quad k \in \{l, r\},$$

where $b_{(i,k)}$ is the left/right monocular subfield of neuron i. The contrast estimate x_k of the left and right subfield of the input image is separately processed by two contrast units

$$y(x_k) = \frac{m}{1-\theta}[x_k - \theta]_+.$$

As the contrast estimate x_k crosses the threshold θ, the output $y(x_k)$ increases from zero until it saturates at m. We chose the threshold $\theta = 0.6$, just above perfect binocular input at $x_k = 0.5$ to provide some margin before the self-reinforcing feedback loop becomes active (Fig. 5B). Further, we set the saturation $m = 0.8$ to prevent total suppression of one eye. Finally, the subsequent input sub-patches for the cortical coder are adjusted to

$$R_k(t) \leftarrow R_k(t)\left(1 + y(x_k(t-1)) - y(x_{\bar{k}}(t-1))\right).$$

Software and Documentation. Documented MATLAB® code of the model will be made available after publication

ACKNOWLEDGMENTS. This work was supported by the German Federal Ministry of Education and Research under Grants 01GQ1414 and 01EW1603A, the Hong Kong Research Grants Council under Grant 618713, and the Quandt Foundation. We thank Maria Fronius and Rowan Candy for numerous discussions.

1. Clark DD, Sokoloff L (1999) Circulation and energy metabolism of the brain in *Basic Neurochemistry: Molecular, Cellular and Medical Aspects*, eds. Siegel GJ, Agranoff BW, Albers RW, Fisher SK, Uhler MD. (Lippincott-Raven, Philadelphia), p. 637–670.
2. Barlow HB, , et al. (1961) Possible principles underlying the transformation of sensory messages. *Sensory communication* 1:217–234.
3. Simoncelli EP, Olshausen BA (2001) Natural image statistics and neural representation. *Annual review of neuroscience* 24(1):1193–1216.
4. Lewicki MS (2002) Efficient coding of natural sounds. *Nature neuroscience* 5(4):356.
5. Atick JJ, Redlich AN (1992) What does the retina know about natural scenes? *Neural computation* 4(2):196–210.
6. Olshausen BA, Field DJ (1997) Sparse coding with an overcomplete basis set: A strategy employed by v1? *Vision research* 37(23):3311–3325.
7. Wiesel TN, Hubel DH (1963) Single-cell responses in striate cortex of kittens deprived of vision in one eye. *Journal of neurophysiology* 26(6):1003–1017.
8. Hirsch HV, Spinelli D (1970) Visual experience modifies distribution of horizontally and vertically oriented receptive fields in cats. *Science* 168(3933):869–871.
9. Movshon JA, Van Sluyters RC (1981) Visual neural development. *Annual review of psychology* 32(1):477–522.
10. Espinosa JS, Stryker MP (2012) Development and Plasticity of the Primary Visual Cortex. *Neuron* 75(2):230–249.
11. Zhao Y, Rothkopf CA, Triesch J, Shi BE (2012) A unified model of the joint development of disparity selectivity and vergence control in *Development and Learning and Epigenetic Robotics (ICDL), 2012 IEEE International Conference on*. (IEEE), pp. 1–6.
12. Teulière C, et al. (2015) Self-calibrating smooth pursuit through active efficient coding. *Robotics and Autonomous Systems* 71:3–12.
13. Gibson JJ (1966) *The Senses Considered as Perceptual Systems*. (Boston, USA: Houghton Mifflin).
14. Friston K, Thornton C, Clark A (2012) Free-energy minimization and the dark-room problem. *Frontiers in psychology* 3:130.
15. Sims A (2017) The problems with prediction in *Philosophy and Predictive Processing*, eds. Metzinger TK, Wiese W. (MIND Group, Frankfurt am Main).
16. Tondel GM, Candy TR (2008) Accommodation and vergence latencies in human infants. *Vision research* 48(4):564–576.
17. Blakemore C, Van Sluyters RC (1974) Experimental analysis of amblyopia and strabismus. *The British journal of ophthalmology* 58(3):176.
18. Kenyon RV, Ciuffreda K, Stark L (1980) Dynamic vergence eye movements in strabismus and amblyopia: symmetric vergence. *Investigative ophthalmology & visual science* 19(1):60–74.
19. Manh V, Chen AM, Tarczy-Hornoch K, Cotter SA, Candy TR (2015) Accommodative performance of children with unilateral amblyopia. *Investigative ophthalmology & visual science* 56(2):1193–1207.
20. Levi DM, Knill DC, Bavelier D (2015) Stereopsis and amblyopia: a mini-review. *Vision research* 114:17–30.
21. Stryker MP, Loewel S (2018) Amblyopia: New molecular/pharmacological and environmental approaches. *Visual neuroscience* 35.
22. Cotter SA, Group PEDI, , et al. (2006) Treatment of anisometropic amblyopia in children with refractive correction. *Ophthalmology* 113(6):895–903.
23. Steele AL, et al. (2006) Successful treatment of anisometropic amblyopia with spectacles alone. *Journal of American Association for Pediatric Ophthalmology and Strabismus* 10(1):37–43.
24. Zhu Q, Triesch J, Shi BE (2017) Joint learning of binocularly driven saccades and vergence by active efficient coding. *Frontiers in neurorobotics* 11:58.
25. Klimmasch L, Lelais A, Lichtenstein A, Shi BE, Triesch J (2017) Learning of active binocular vision in a biomechanical model of the oculomotor system in *2017 Joint IEEE International Conference on Development and Learning and Epigenetic Robotics (ICDL-EpiRob)*. (IEEE), pp. 21–26.
26. Hunt JJ, Dayan P, Goodhill GJ (2013) Sparse Coding Can Predict Primary Visual Cortex Receptive Field Changes Induced by Abnormal Visual Input. *PLoS Computational Biology* 9(5).
27. Sherman SM, Stone J (1973) Physiological normality of the retina in visually deprived cats. *Brain Research* 60(1):224–230.
28. Movshon JA, et al. (1987) Effects of early unilateral blur on the macaque's visual system. iii. physiological observations. *Journal of Neuroscience* 7(5):1340–1351.
29. Yoshioka T, Blasdel GG, Levitt JB, Lund JS (1996) Relation between patterns of intrinsic lateral connectivity, ocular dominance, and cytochrome oxidase-reactive regions in macaque monkey striate cortex. *Cerebral Cortex* 6(2):297–310.
30. Iacaruso MF, Gasler IT, Hofer SB (2017) Synaptic organization of visual space in primary visual cortex. *Nature* 547(7664):449–452.
31. Moradi F, Heeger DJ (2009) Inter-ocular contrast normalization in human visual cortex. *Journal of Vision* 9(3):13–13.
32. Said CP, Heeger DJ (2013) A model of binocular rivalry and cross-orientation suppression. *PLoS computational biology* 9(3):e1002991.
33. Carandini M, Heeger DJ (2012) Normalization as a canonical neural computation. *Nature Reviews Neuroscience* 13(1):51.
34. Chen L, Kruger PB, Hofer H, Singer B, Williams DR (2006) Accommodation with higher-order monochromatic aberrations corrected with adaptive optics. *Journal of the Optical Society of America. A, Optics, image science, and vision* 23(1):1–8.
35. Zannoli M, Love GD, Narain R, Banks MS (2016) Blur and the perception of depth at occlusions. *Journal of Vision* 16(6):17–17.
36. Bharadwaj SR, Candy TR (2009) Accommodative and vergence responses to conflicting blur and disparity stimuli during development. *Journal of vision* 9(11):4.1–18.
37. Bharadwaj SR, Candy TR (2011) The effect of lens-induced anisometropia on accommodation and vergence during human visual development. *Investigative Ophthalmology and Visual Science*.
38. Holopigian K, Blake R, Greenwald MJ (1986) Selective losses in binocular vision in anisometropic amblyopes. *Vision research* 26(4):621–630.
39. Babu RJ, Clavagnier S, Bobier WR, Thompson B, Hess RF (2017) Regional extent of peripheral suppression in amblyopia. *Investigative Ophthalmology and Visual Science* 58(4):2329–2340.
40. Bradley A, Freeman RD (1981) Contrast sensitivity in anisometropic amblyopia. *Investigative Ophthalmology and Visual Science* 21(3):467–476.
41. Evans BJ (2007) Monovision: A review. *Ophthalmic and Physiological Optics* 27(5):417–439.
42. Hess RF, Thompson B (2015) Amblyopia and the binocular approach to its therapy. *Vision Research* 114:4–16.
43. Hallum LE, et al. (2017) Altered balance of receptive field excitation and suppression in visual cortex of amblyopic macaque monkeys. *The Journal of Neuroscience* 37(34):8216–8226.
44. Kehrein S, Kohnen T, Fronius M (2016) Dynamics of interocular suppression in amblyopic children during electronically monitored occlusion therapy: first insight. *Strabismus* 24(2):51–62.
45. Schor CM, Alexander J, Cormack L, Stevenson S (1992) Negative feedback control model of proximal convergence and accommodation. *Ophthalmic and Physiological Optics* 12(3):307–318.
46. Hoyer PO, Hyvärinen A (2000) Independent component analysis applied to feature extraction from colour and stereo images. *Network: computation in neural systems* 11(3):191–210.
47. Gibaldi A, Chessa M, Canessa A, Sabatini SP, Solari F (2010) A cortical model for binocular vergence control without explicit calculation of disparity. *Neurocomputing* 73(7-9):1065–1073.
48. Gibaldi A, Canessa A, Sabatini SP (2017) The active side of stereopsis: Fixation strategy and adaptation to natural environments. *Scientific reports* 7:44800.
49. Rao RP, Ballard DH (1999) Predictive coding in the visual cortex: a functional interpretation of some extra-classical receptive-field effects. *Nature neuroscience* 2(1):79.
50. Friston K (2010) The free-energy principle: a unified brain theory? *Nature reviews neuroscience* 11(2):127.
51. Palmer SE, Marre O, Berry MJ, Bialek W (2015) Predictive information in a sensory population. *Proceedings of the National Academy of Sciences* 112(22):6908–6913.
52. Olmos A, Kingdom FA (2004) A biologically inspired algorithm for the recovery of shading and reflectance images. *Perception* 33(12):1463–1473.
53. Mallat SG, Zhang Z (1993) Matching pursuits with time-frequency dictionaries. *IEEE Transactions on signal processing* 41(12):3397–3415.
54. Bhatnagar S, Sutton R, Ghavamzadeh M, Lee M (2009) Natural actor-critic algorithms. *Automatica* 45(11).
55. Hubel DH, Wiesel TN (1962) Receptive fields, binocular interaction and functional architecture in the cat's visual cortex. *The Journal of physiology* 160(1):106–154.
56. Adelson EH, Bergen JR, , et al. (1991) *The plenoptic function and the elements of early vision*. (Vision and Modeling Group, Media Laboratory, Massachusetts Institute of . . .).
57. Chung HW, Sadler BM, Hero AO (2017) Bounds on variance for unimodal distributions. *IEEE Transactions on Information Theory* 63(11):6936–6949.